# The Wavenumber Shift in SAR Interferometry

Fabio Gatelli, Andrea Monti Guarnieri, Francesco Parizzi, Paolo Pasquali, Claudio Prati, and Fabio Rocca

*Abstract*—**SAR surveys from separate passes show relative shifts of the ground wavenumber spectra that depend on the local slope and the off-nadir angle. We discuss the exploitation of this spectral shift for different applications: 1) generation of "low noise" interferograms benefiting phase unwrapping, 2) generation of quick-look interferograms, 3) decorrelation reduction by means of tunable SAR systems (TINSAR),[1] 4) range resolution enhancement, and 5) the combination of SAR data gathered by different platforms (airborne and satellite) for a "long-time coherence" study.**

## I. Introduction

SAR interferometry was introduced 20 years ago by Graham [1]. However, only after recent studies in Europe and at the Jet Propulsion Laboratory, has its potential been fully demonstrated. The growing interest in SAR interferometry is also due to the impressive amount of data suitable for interferometry from the first European remote sensing satellite (ERS-1) and the many airborne systems available.

The information added by interferometry to detected SAR images is clearly shown in the example of Fig. 1 and 2. In Fig. 1, the ERS-1 detected image of the area of Naples, Italy is shown. In the upper part, Vesuvius (the large volcano that dominates the area of Naples) is imaged. From this image it is difficult to get an idea of the topography. Fig. 2 shows the interferogram (phase fringes) generated from two repeated ERS-1 surveys. The topography is now evident, since the imaged phase fringes are strictly related to the elevation contour lines.

The relation between the phase of SAR interferograms and ground elevation is usually explained by means of geometrical approaches [2], [3]. They are based on the assumption that the RF bandwidth is so small (and this is the case with most satellite systems, including ERS-1) to be negligible. Thus, the system is considered monochromatic.

This approximation, however, hides an important aspect of the interferogram-generation mechanism. In fact, if the finite system bandwidth is considered, a relative shift of the ground wavenumber spectra dependent on the baseline and the local slope is recognized. Important consequences are revealed from this result.

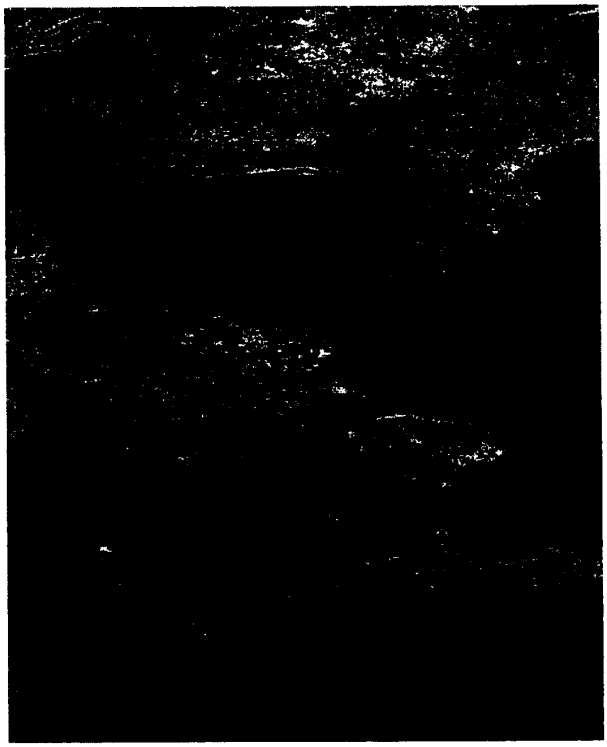

Fig. 1 ERS-1 SAR detected image: Naples and the Vesuvius.

1) It can be shown that as the baseline increases and in the absence of volumetric effects, to be discussed later, only the spatial resolution of the interferogram is reduced since the "geometrical decorrelation" [4] can be removed. Thus, techniques for improving interferogram quality (i.e., yielding a higher SNR) can be found (with a considerable benefit for phase unwrapping). Moreover, this effect could be completely avoided by means of tunable systems.

2) Rules for the design of presumming filters for quick-look interferometric processing can be derived.

3) Repeated satellite surveys can be combined in order to improve the slant range image resolution [7].

In this paper the emphasis is on interferograms generation, quick-look interferometric processing, and tunable interferometric satellite SAR systems. Symbols that will be used throughout the paper are summarized in Table I and Fig. 3.

Manuscript received June 28, 1993; revised February 8, 1994. This work was supported in part by the European Space Agency and by the ESRIN under the FRINGE Project.

The authors are with the Dipartimento di Elettronica, Politecnico di Milano, 20133 Milan, Italy.

IEEE Log Number 9402681.

[1]Patent pending.

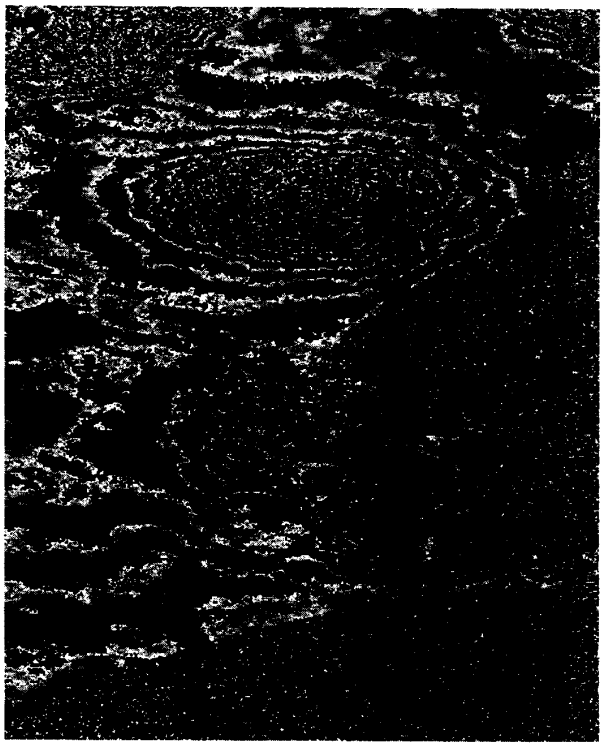

Fig. 2. ERS-1 SAR interferometric fringes: Naples and the Vesuvius volcano.

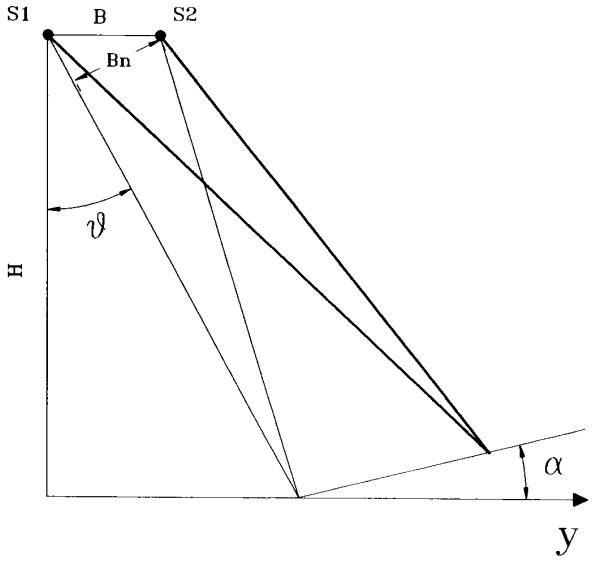


Fig. 3. INSAR geometry (see Table I).

TABLE I
LIST OF SYMBOLS

| Symbol | Meaning | ERS-1 |
|---|---|---|
| $\lambda$ | wavelength | 5.66 cm |
| $f_o = c/\lambda$ | central frequency | 5.3 GHz |
| $\Delta f$ | equivalent frequency shift | |
| $W$ | system bandwidth | 16 MHz |
| $\theta$ | off-nadir angle | 23° |
| $\Delta\theta$ | stereo pair angular separation | |
| $\alpha$ | local terrain slope (range) | |
| $H$ | platform altitude | 780 km |
| $\rho_s$ | slant range resolution | 9.375 m |
| $B$ | horizontal interferometer baseline | |
| $B_n$ | $B$ project. normal to the look direction | |
| $B_{nc}$ | critical baseline | $\simeq$ 1100m for $\alpha = 0$ |
| $B_{nT}$ | critical baseline for TINSAR | |
| $r$ | slant range axis | |
| $r_o$ | sensor-target distance | |
| $y$ | ground range axis | |
| $k_y$ | ground range wave number | |
| $z$ | vertical axis | |
| $k_z$ | vertical wave number | |
| $\phi$ | interferometric phase | |
| $c$ | light velocity | $3 \cdot 10^8$m/s |
| $a(y,z)$ | ground reflectivity | |

## II. Interferogram Generation: The Monochromatic Approach

Let us consider two complex images $v_1$ and $v_2$ from two separate passes and let us suppose that the terrain backscatter did not change.

Let us now exploit the "monochromatic approximation": the relative system bandwidth is so small (i.e., in the ERS-1 case its value is $3 \cdot 10^{-3}$) to be neglected. Thus, the phase difference $\phi$ between the correspondent complex pixels in $v_1$ and $v_2$ is proportional to the travel path difference $2\Delta r_0$:

$$\phi = \frac{4\pi}{\lambda} \Delta r_0. \tag{1}$$

The interferometric phase $\phi$ is usually derived from the phase of the product $v_1 v_2^*$ where the * represents a complex conjugate. In fact, $v_1 v_2^*$ is also a complex image (the interferogram) that has a phase equal to $\phi$. The quality of the interferometric phase depends on the amount of phase noise that, in general, comes from distinct sources [3], [4]:

1) system noise
2) terrain decorrelation (nonsimultaneous surveys)
3) image misregistration
4) approximate focusing
5) "geometric decorrelation."

As far as the last source of noise is concerned, it has been said [4] that it increases with the baseline. In fact,

this source of phase error is also referred as the "baseline decorrelation error." It has also been shown [2], [3] that the total baseline decorrelation is reached in correspondence with the critical baseline:

$$|B_{nc}| = \left|\frac{\lambda \cdot r_0 \cdot \tan(\theta - \alpha)}{2\rho_s}\right|. \quad (2)$$

In the next section it will be shown that the geometric decorrelation concept without reference to volumetric scatter phenomena is in some ways misleading; we shall see that the decorrelation noise of flat scatterers can easily be avoided with a suitable interferogram formation technique.

## III. Interferogram Generation: The Spectral Approach

In [7], it has been shown that the spectra of the signals $v_1$ and $v_2$ correspond to different bands of the ground reflectivity's spectrum.

That point can be easily demonstrated starting from the approximated relation between the frequency $f$ and the ground range wavenumber $k_y$:

$$k_y = \frac{4\pi}{\lambda}\sin(\theta - \alpha) = \frac{4\pi f}{c}\sin(\theta - \alpha). \quad (3)$$

Here, for the sake of simplicity, we have considered a constant uniform slope $\alpha$ of the terrain. $\Delta k_y$, i.e., the variation of $k_y$ generated by a slight change of the looking-angle $\Delta\theta$, follows:

$$\Delta k_y = \frac{4\pi f \Delta\theta}{c}\cos(\theta - \alpha). \quad (4)$$

Thus, in general, a looking-angle difference $\Delta\theta$ generates a shift and a stretch of the imaged terrain spectra. However, if the relative system bandwidth is small, the frequency $f$ in the second term of (4) can be substituted with the central frequency $f_0$. The stretch can be neglected and the following equation holds:

$$\Delta k_y = \frac{4\pi f_0 \Delta\theta}{c}\cos(\theta - \alpha). \quad (5)$$

Finally, since the radar is not monochromatic (we have a bandwidth $W$ centered around the central frequency $f_0$), we can conclude that by changing the looking angle of the SAR survey, we get a different band of the ground reflectivity spectrum.

Now, in order to compare the shift of the ground reflectivity spectrum to the SAR bandwidth $W$, it is worth expressing the ground wavenumber shift of (5) as an equivalent frequency shift $\Delta f$. The following expression of $\Delta f$ for an angular separation $\Delta\theta$ can be obtained by differentiation of (3) directly:

$$\Delta f = -\frac{f_0 \Delta\theta}{\tan(\theta - \alpha)} = -\frac{cB_n}{r_0 \lambda \tan(\theta - \alpha)}. \quad (6)$$

We would like to stress again that (6) does not state that by changing the looking angle of the SAR survey the radar bandwidth is shifted by $\Delta f$. It just says that by changing the SAR looking angle, the backscattered signal contains different spectral components of the ground reflectivity spectrum. In other words, if we look at the signals received by two SARs separated by an angle $\Delta\theta$, (6) states that the same spectral components of the first signal are found in the second spectrum shifted by $\Delta f$. In substance, it is the optical diffraction gratings idea, one that goes back to the eighteenth century.

A similar result can be demonstrated for the bistatic SAR case (but not the ERS-1 case). In that case, a stereo pair is acquired simultaneously by two sensors: the first is equipped with a transmitter and a receiver, whereas the second is equipped with a receiver only. It can be shown that the spectral shift induced by a baseline $B_n$ is half that obtained in the monostatic case:

$$\Delta f = -\frac{cB_n}{2r_0 \lambda \tan(\theta - \alpha)}. \quad (7)$$

Finally, note that in the monostatic case the two SAR spectra become totally disjoint as the frequency shift $\Delta f$ equals the system bandwidth $W$. From (6) the critical baseline can be computed as

$$|B_{nc}| = \left|\frac{W r_0 \lambda \tan(\theta - \alpha)}{c}\right|. \quad (8)$$

Then, since $W = c/(2\rho_s)$, the expression of the critical baselines (8) is identical to that of (2). The spectral shift equation (6) can be used for different applications.

### A. Improvement of the Interferogram SNR

If the signals $v_1(n)$ and $v_2(n)$ are sampled correctly, the interferogram's spectrum $R(k)$ is the linear cross-correlation of the two spectra $V_1(k)$ and $V_2(k)$. Let us consider that the reflectors are located on a constant slope $\alpha$, for the sake of simplicity. In the following, we shall refer to the reflectivity's spectrum common to both SAR spectra as the "common band." The linear cross-correlation of the spectra shows three distinct contributions:

1) a peak at the frequency shift $\Delta f$, for which the common bands coincide (the "signal"). Note that $\Delta f$ from (6) is identical to the interferogram fringe frequency;

2) a random sequence coming from the cross-correlation of the common bands other than in the peak position. This sequence is conjugate symmetric around the peak position and the phase of its inverse Fourier transform is linear. This term is responsible for the magnitude fluctuation of the interferogram, but does not create phase disturbances unless the symmetry is not broken by filtering the interferogram;

3) a second random sequence coming from the cross-correlation of the disjoint parts of the spectra ("noise").

As stated in [7]–[9], it is clear that the noise contribution 3) can be easily avoided by prefiltering the components of the two signals $v_1$ and $v_2$. The following expressions of the filter bandwidth $W_f$ and central frequencies $f_1$

and $f_2$ hold:

$$W_{f1} = W_{f2} = W - \Delta f \tag{9}$$

$$f_1 = \frac{\Delta f}{2} \tag{10}$$

$$f_2 = -\frac{\Delta f}{2}. \tag{11}$$

As for practical cases, the constant slope assumption is generally not respected and range varying filters have to be used. Their bandwidths and central frequencies can be estimated from the fringes of a noisier interferogram generated without filtering.

The example of Fig. 4 shows the fringe's (interferogram phase) SNR enhancement that is obtained in the ERS-1 case with a baseline of 600 m (the noise that is still present is coming mainly from the image's decorrelation in time). Therefore, the spectral bandwidth of the interferogram is reduced (with no loss of spatial resolution), and the geometric decorrelation is removed. A quantitative measurement of the enhancement is shown in Fig. 5, where the coherence histogram is shown.

Fig. 4. Interferogram SNR enhancement that is obtained in the ERS-1 case with a baseline of 600 m: Bonn area.

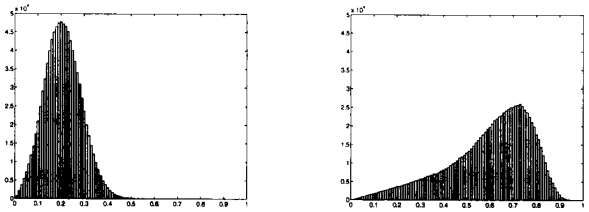

Fig. 5. Coherence histogram of the two SAR images used to generate the interferogram of Fig. 4. Left-hand side: before filtering. Right-hand side: after filtering

### *B. Effect of Volume Scattering: The Baseline as an Additional Dimension*

Up to now, we have considered only surface scattering, neglecting the effect of volume scattering [4], [5]. However, when backscattering comes from targets with a different elevation $z$ within the resolution cell, volume effects cannot be ignored.

This case is shown in Fig. 6(a): the scatterers are contained in a box with the dimensions $(\Delta y, \Delta z)$, (the problem can be assumed to be invariant with respect to the azimuth direction). The radar return is a function of the complex reflectivity $a(y, z)$, the radio frequency $\omega = 2\pi f$, and the looking-angle $\theta$.

$$A(\omega, \theta) = \iint a(y, z) \cdot \exp\left[-j\frac{2\omega}{c}(y \sin\theta - z\cos\theta)\right] dy\, dz. \tag{12}$$

We consider the medium as semitransparent, in the usual first-Born approximation, so that the scattered signal is a linear superposition of effects. Wavenumbers in the ground range $k_y$ and now in elevation $k_z$ as well, have the following form:

$$|k_y| = \frac{2\omega}{c}\sin\theta$$

$$|k_z| = \frac{2\omega}{c}\cos\theta. \tag{13}$$

The following expression of the received signal holds:

$$A(k_y, k_z) = \iint a(y, z)\exp\left[-j(k_y y + k_z z)\right] dy\, dz. \tag{14}$$

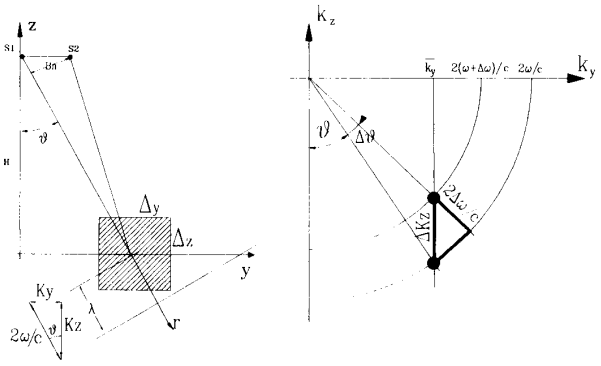


Fig. 6. Volumetric scattering. (a) Left-hand side: geometry. (b) Right-hand side: wavenumber representation.

Thus, the received signal can be regarded as the 2-D Fourier transform of the ground reflectivity measured at the wavenumbers given by (13).

Two SAR surveys from different angles ($\theta$ and $\theta + \Delta\theta$) represent different bands of the complex reflectivity spectrum. From Fig. 6(b), it is clear that in order to observe the same $k_y$ from the two surveys (i.e., the condition that allows coherent interferometry in the case of surface scattering), the looking-angle change $\Delta\theta$ should be compensated by the spectral shift $\Delta\omega = -\omega\Delta\theta/\tan(\theta)$ that is equivalent to the following $k_z$ wavenumber shift: $\Delta k_z \simeq -2\Delta\omega/(c\cos\theta) = 2\omega\Delta\theta/(c\sin\theta)$.

The coherence of the interferometric surveys depends on the degree of spectral correlation between the measurements in $k_z$ and $k_z + \Delta k_z$. If we consider, as a special case, the flat box ($\Delta z = 0$), the signal is impulsive in the

$z$ domain and we have total correlation of the different spectral components and unitary coherence. In general, with a finite volume and a nonzero value of $\Delta z$, we shall have the following expression of the spectral correlation function:

$$\frac{\sin(\Delta k_z \Delta z/2)}{\Delta k_z \Delta z/2}.$$

Therefore, we can state that whenever $|\Delta z| \ll 2\pi/|\Delta k_z|$, the volumetric effects can be neglected. A useful expression can be found as a function of transmitted wavelength, normal baseline, and satellite altitude:

$$|\Delta z| \ll \left|\frac{\lambda H \tan\theta}{2B_n}\right| = |\Delta z_0|. \tag{15}$$

If we consider the case of $|\Delta z| \geq |\Delta z_0|$, we have spectral decorrelation and low coherence. In the ERS-1 case with a baseline of 250 m, decorrelation is expected for $|\Delta z| \geq$ 38 m. On the other hand, one might claim that this is not decorrelation but signal. One could reasonably consider the change of the two SAR images usable as a function of the baseline (the difference of the complex samples) as signal.

For the sake of simplicity let us use the following approximation:

$$\begin{aligned} A(k_y, k_z + \Delta k_z) &\simeq A(k_y, k_z) + \frac{\partial A}{\partial k_z} \cdot \Delta k_z \\ &= A(k_y, k_z) - \frac{j\,2\omega\Delta\theta}{c \sin\theta} \int\int za(y, z) \\ &\quad \cdot \exp[-j(k_y y + k_z z)]\, dy\, dz \\ &= A(k_y, k_z) - \frac{j\,4\pi B_n}{H\lambda \tan\theta} V(k_y, k_z). \end{aligned} \tag{16}$$

Here, $V(k_y, k_z)$ is the result of the double integral. Thus, if we have many interferometric observations with different baselines, we can split each observation $A_i(k_y, k_z)$ into a "surface contribution" $A(k_y, k_z)$ and a "volumetric contribution" proportional to the baseline; this term is proportional to the moment of the reflectivity along the $z$ axis:

$$A_i(k_y, k_z) = A(k_y, k_z) - \frac{j\,4\pi B_n}{H\lambda \tan\theta} V(k_y, k_z). \tag{17}$$

From those observations, it is then possible to derive an LMS estimate of the surface and the volumetric contributions. Just as an example, six ERS-1 surveys of the Bonn area have been exploited for this goal after registration in space and frequency. The estimated surface and volumetric contributions are shown in Fig. 7. They are not represented with the same scale, since the average amplitude of the surface contribution is roughly 20 times that of the volumetric contribution. As of yet, no definitive conclusions have been derived from this example. For one, it can be noted that the volumetric contribution shows sidelobes extended in the range direction (vertical in the image). This feature comes from sidelobes of strong point scatterers laying on adjacent range bins. Due to the spectral shift compensation, the sidelobes are phase shifted with respect to the main lobe, proportional both to the baseline and to their distance from the main lobe. Hence, they tend to be canceled from the surface contribution, but less so from the volumetric contribution, as far as the linear dephasing approximates a linear change proportional to the baseline. Different results could be obtained by regressing with the baseline phase and modulus instead of real and imaginary parts, as has been done in this example. The concepts have been checked with synthetic examples that for brevity are not reported here and could be further tested by means of controlled experiments (e.g., by exploiting the new anechoic chamber available at JRC-EMSL [6]).

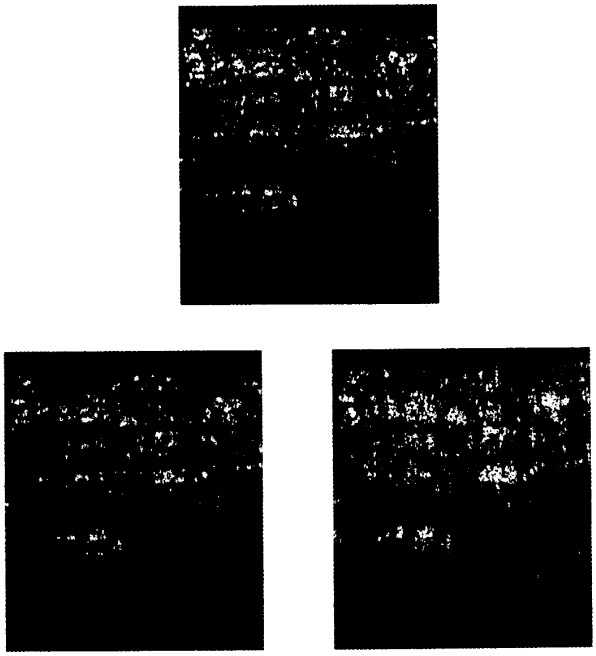

Fig. 7. Volume scattering. Six ERS-1 images (area of Bonn) have been processed to separate common parts and volumetric effects. Top: one of the images. Left-handside: common parts. Right-hand side: volumetric contributions. Image size: 1 km, azimuth (horizontal) × 2 km, range (vertical).

### C. Separation of Layover Areas

The spectral shift between the two passes given in (6) shows a dependence upon the local terrain slope along range $\alpha$. As the local slope approaches the off-nadir angle, the spectra become disjoint (blind angles) and finally, the spectral shift goes to infinity. If the local slope increases again (layover) the absolute value of the spectral shift decreases, but the sign is changed. As a consequence, negative and positive frequencies of the interferogram spectrum refer to areas of layover and nonlayover, respectively. Therefore, they can be separated, provided that the time span of the layover slope is long enough

(i.e., enough slant range samples are available for frequency estimation and filtering). In Fig. 8 the spectral shift as a function of the local slope is shown in the case of ERS-1, with a baseline of 600 m and a nominal off-nadir angle of 23°. An example of layover separation with ERS-1 data of a mountainous area in Switzerland is shown in Fig. 9. It is worth noting that there are cases where only a partial separation can be achieved. A typical example is represented by a step function along the range direction. In such a case, we would have three contributions from different regions summed at the same interferogram position: the first flat zone at the lower elevation, the second flat zone at the higher elevation, and the step transition. The step transition can be separated from the other two since it shows a different frequency of the fringes. However, the two flat zones show the same spectral shift and cannot be separated other than using ascending and descending passes. The step area would be in a shadow.

If layover areas could be separated from the rest of the image, slopes in the range direction from 36° to 90° (together with those from −67° to 9.7°) could be recovered by ERS-1 SAR interferometry with ground resolution dependent on slope, as usual. Moreover, by exploiting both ascending and descending ERS-1 passes, almost all slopes from −90° to +90° with whatever azimuth orientation are recovered; this situation is shown in Figure 10. The different curves of Fig. 10 identify the slopes $\alpha$ recoverable from ERS-1 (see Fig. 8) as a function of their azimuth orientation (see the lower part of Fig. 10). Thick and thin lines refer to ascending and descending passes, respectively.

Here, the few combinations of slope and azimuth orientation that could not be recovered from ERS-1 data are shown (black areas). On the other hand, if we were not able to deal with layover areas, the nonobservable combinations would be more (the shaded areas).

### D. A Tunable Interferometric SAR System

A tunable interferometric SAR (TINSAR) would allow one to overcome one of the most serious limitations in generating interferograms from multiple SAR surveys: the loss of coherence due to large baselines.

*1) Monostatic, Two Passes:* In Section III, it has been shown that by changing the looking angle of the SAR survey, a different band of the ground reflectivity spectrum is recovered. Thus, as an example, baselines larger than say, 1 km, would not be usable for ERS-1 interferometry. On the other hand, as suggested by (6), the equivalent frequency shift induced by a 1 km baseline could be compensated by shifting the central transmit frequency during the second survey by 15 MHz. This could be done by means of a tunable transmitter with the central frequency shifted proportional to the estimated baseline, following (6). In this way, baselines larger than that allowed by a fixed frequency radar could be exploited and, consequently, less stringent requirements on the satellite maneuver accuracy would be required.

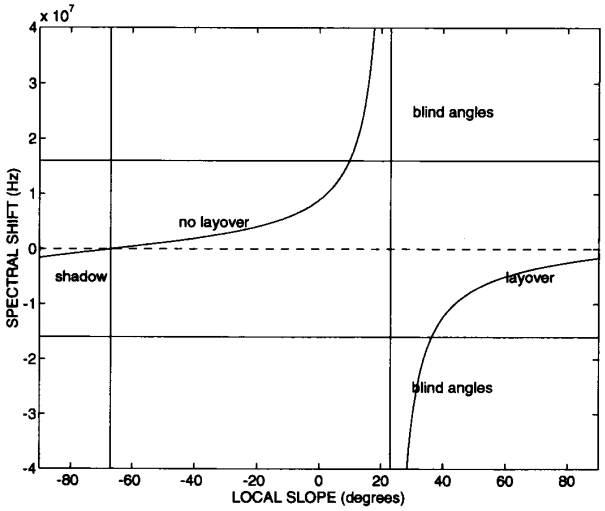


Fig. 8. Spectral shift as a function of the local slope in the case of ERS-1 with a baseline of −600 m and a nominal off-nadir angle of 23°. Blind angles: from 9.7 to 36.2°. The two horizontal continuous lines limit the usable spectral shift (±16 MHz).

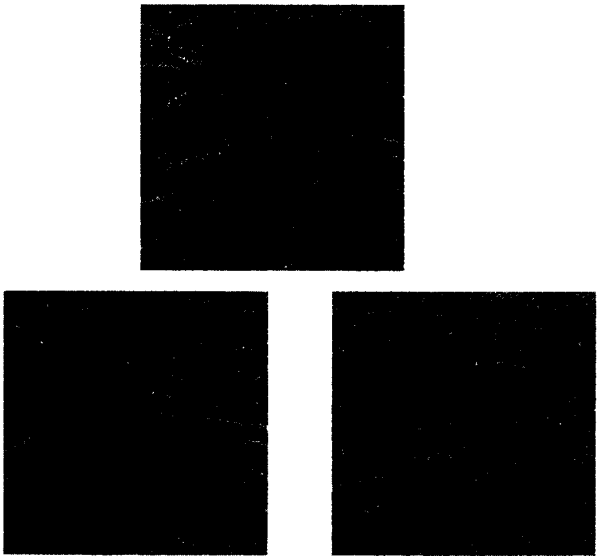

Fig. 9. Layover separation with ERS-1 data of a mountainous area near Luzern, Switzerland. Top: fringes. Left-hand side: fringes of nonlayover areas. Right-hand side: fringes of layover areas.

*2) Bistatic, One Pass:* In the case of a bistatic interferometric system there is only one transmitter, but two receivers. Therefore, in order to achieve the requested spatial resolution and a total spectral correlation over the receiver's bandwidth $W$, the transmitter bandwidth must be larger than $W$. The same bandwidth $W$ centered around two carrier frequencies separated by $\Delta f$ [as computed from (7)] must be transmitted in such a way that the images of a flat topography are consistent over the entire frequency band.

If the spectral shift $\Delta f$ is smaller than $W$, the two trans-

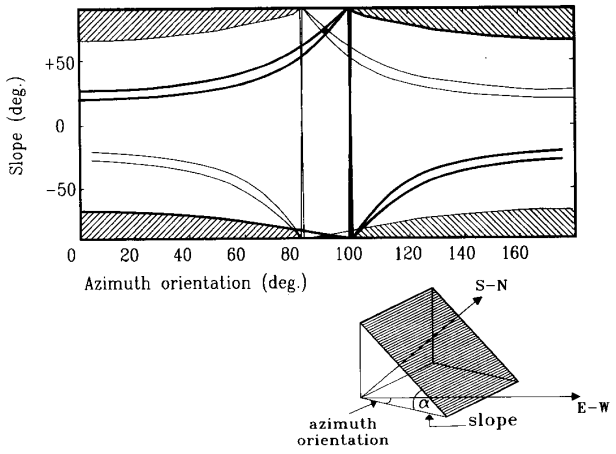


Fig. 10. Combinations of slope and azimuth orientation that cannot be recovered from ERS-1 data. With layover separation (black areas). Without layover separation (shaded areas).

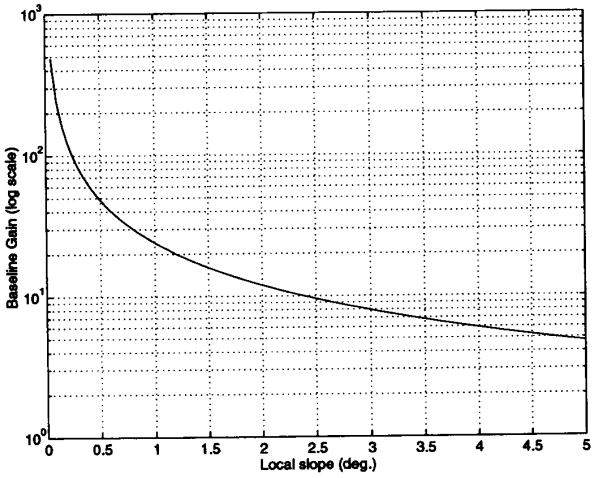


Fig. 11. Baseline gain as a function of the local slope.

mitted bands would overlap. In such a case, of course, a larger bandwidth would suffice.

*3) Advantages Offered by the TINSAR:* The use of the TINSAR would be particularly advantageous (with respect to a fixed frequency INSAR) when a smooth topography has to be measured with single-pass interferometry (gently sloping areas, sea surfaces, and so forth). Since the slope deviation with respect to a reference flat surface is modest, a large baseline must be adopted in order to have a phase deviation significantly larger than the plane noise. On the other hand, the baseline is limited by the largest local terrain slope $\alpha$. From (7), if the largest allowed spectral shift is say, $W/4$ (one-fourth of the RF bandwidth), the baseline $B_n$ is limited by the local slope as

$$B_n = \frac{r_0 \lambda W}{2c} \tan(\theta - \alpha). \tag{18}$$

In the TINSAR case, (7) is modified in order to compensate the spectral shift in case of flat terrain (in practice it can be achieved by changing the frequency transmitted by the second radar):

$$\Delta f = \frac{f_0 \Delta\theta}{2 \tan(\theta - \alpha)} - \frac{f_0 \Delta\theta}{2 \tan(\theta)} = \frac{cB_n}{2r_0\lambda}\left(\frac{1}{\tan(\theta - \alpha)} - \frac{1}{\tan\theta}\right). \tag{19}$$

In this case, the baseline $B_{nT}$ is limited to

$$B_{nT} = \frac{r_0 \lambda W}{2c} \frac{\tan(\theta - \alpha)\tan\theta}{\tan\theta - \tan(\theta - \alpha)}. \tag{20}$$

The usable baseline can be significantly larger (as can the phase deviation) if TINSAR is adopted. By taking the ratio between (18) and (20), the gain in the baseline is

$$G = \frac{B_{nT}}{B_n} = \frac{\tan\theta}{\tan\theta - \tan(\theta - \alpha)}. \tag{21}$$

The gain as a function of the local slope is shown in Fig. 11.

The TINSAR principle could also be used for multipass airborne SAR interferometry (typically for differential interferometry applications). For that case it is of interest to derive the expression of the spectral shift as a function of the off-nadir angle and the correspondent shift of the line of flight (the broadside SAR). After some simple algebra from (6) the following holds:

$$\Delta f = \frac{B \cos^3\theta f_0}{H \sin\theta}. \tag{22}$$

The spectral shift as a function of $\theta$ is shown in Fig. 12 for $f_0 = 1$, 5, and 20 GHz, $H = 10$ km, and $B = 1$ m. In section III-G, an experiment will be proposed to exploit the wide coverage of wavenumbers offered by wideband airborne SAR.

### *E. Interferometric Quick Look*

The quick-look SAR processing is generally achieved by focusing a data set previously subsampled after presumming. In the case of interferometric processing, range presumming must be designed taking case of a few simple rules that arise again from the spectral shift equation (6). Let us refer again to the ERS-1 case and let us suppose that the requested ground resolution is 50 × 50 m. The "full bandwidth" data set can be subsampled by a factor of two in the range (and by a higher factor in azimuth that is not essential for the present discussion). If interferometric capabilities are not requested, a half-band low-pass filter can be applied to the data before subsampling (in practice, filtering and subsampling are performed at the same time). On the other hand, if the common band of the two surveys must be preserved, the low-pass filter must be substituted with half-band band-pass filters with central frequencies $-\Delta f/2$ and $+\Delta f/2$ for the first and second data sets, respectively. As an example, a 40 × 80 km ERS-1 interferometric quick look of the Bonn area

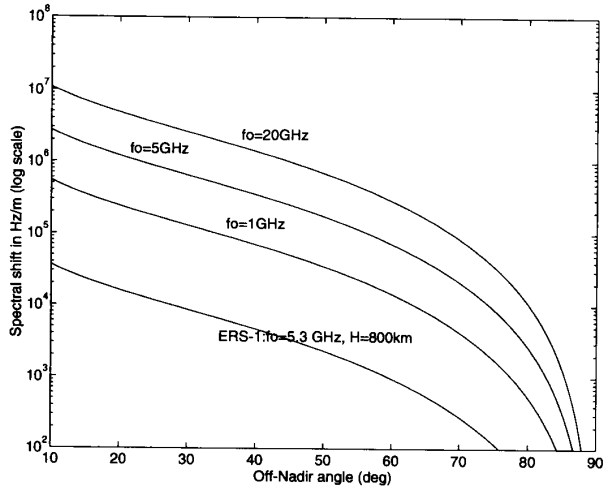


Fig. 12. Spectral shift induced by a 1 m baseline as a function of the off-nadir angle $\theta$ with $f_0$ = 1, 5, and 20 GHz and $H$ = 10 km. The ERS-1 case is shown for comparison.

with a resolution of 50 × 50 m obtained with a baseline of 200 m is shown in Fig. 13.

### F. Improvement of the Slant Range Resolution

Across-track resolution of a spaceborne SAR system is limited by power and data rate constraints. It could be improved if a larger band of the reflectivity's spectrum is recovered. As has been demonstrated in [7], this can be done by properly combining SAR surveys of nearly flat areas derived from separate passes. In fact, due to the spectral shift equation (6), the reflectivity's spectrum band sensed in separate surveys is larger than that of a single survey. Therefore, across-track resolution can be improved by shifting in frequency and in phase one signal with respect to the other and then adding the two. If the spectra of the different surveys partially overlap, the phase of the interferometric signal can be used for estimating the correct phase and frequency shift. It is clear that the larger the frequency shift, the greater the resolution improvement; meanwhile, the phase estimation is less robust. As an example, five repeated ERS-1 surveys, during the three-day repetition cycle from March 2 to 14, of Bonn have been exploited to double the resolution along the range. The comparison between the single survey and the multipass combination is shown in Fig. 14. From this figure, two effects are visible:

1) the range resolution enhancement of fixed targets (see the map of the imaged area in Fig. 15 and the plot of two point scatterers, before and after image combinations in Fig. 16);

2) the relative reduction of the image intensity on areas that decorrelate from one survey to another.

Finally, it is worth mentioning that a spectral shift can also occur in the azimuth direction due to different Doppler centroid frequencies. In such a case, resolution improvement can be applied in the azimuth direction as well (the well-known spot-light effect [10]).

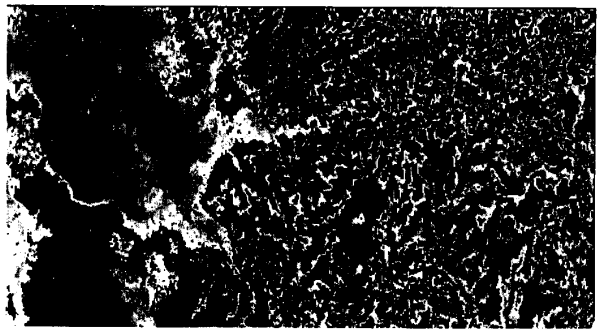

Fig. 13. ERS-1 interferometric quick look of the area of Bonn (40 × 80 km, azimuth range) with a resolution of 50 × 50 m obtained with a baseline of 200 m.

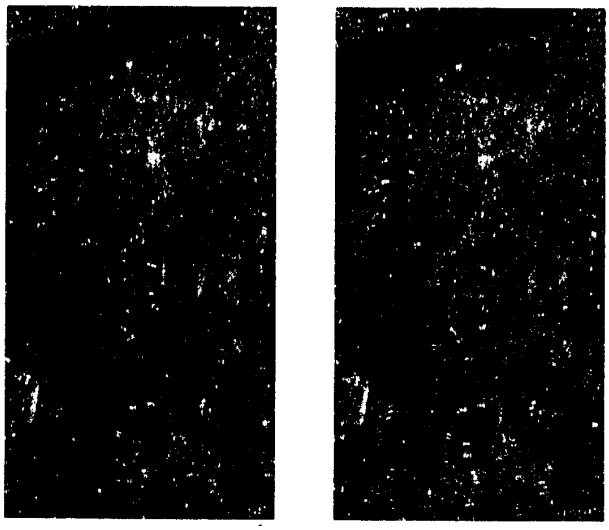

Fig. 14. Range resolution improvement achieved with ERS-1 repeated surveys of Bonn. Left-hand side: single survey. Right-hand side: multiple surveys combination. The pixel dimension is 2 × 2 m.

### G. Combination of SAR Data from Different Platforms

The spectral shift concept is the simplest way to understand how to combine SAR data derived from different SAR systems in order to generate interferograms. As an example, it is of interest to generate interferograms by combining SEASAT (1979) and airborne $L$-band SAR data, since such an experiment would allow study of the $L$-band coherence after a 15-year time interval.

The geometry of the experiment is shown in Fig. 17. Here, we have indicated with $S$ and $A$ the SEASAT and airborne positions, respectively; with $\theta_s$ and $\theta_a$ the SEASAT and airborne SAR looking angles, respectively. Moreover, a nearly flat area such as Death Valley has been hypothesized. The spectral shift concept will be adopted in order to derive the expected result and the airborne SAR track and attitude constraints.

Even if it is not strictly required, let us suppose for the sake of simplicity, that the two SAR's have the same central frequency. From the relationship between the angular


Fig. 15. Map of the imaged area of Bonn.

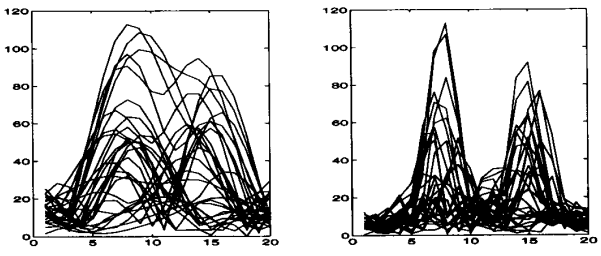

Fig. 16. Plot of two point scatterers. The horizontal axis is range. Several range lines for different azimuth positions are plotted. Left-hand side: single survey. Right-hand side: multiple surveys combination.

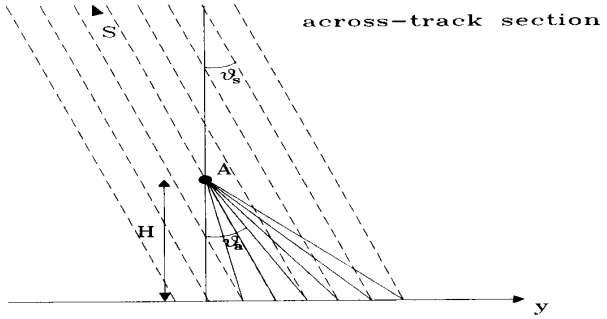


Fig. 17. Geometry of the proposed experiment.

separation and the spectral shift equation (6) it is clear that for $\theta_a = \theta_s$ the two ground reflectivity spectra (derived from SEASAT and the airborne SAR) are centered at the same wavenumber (ground frequency). In that case, since the airborne SAR has a larger bandwidth (100 MHz) with respect to that of SEASAT (20 MHz), the ground reflectivity spectrum collected by SEASAT is totally contained in that collected by the airborne. Thus, if we have coherence after 15 years, an interferogram can be generated.

However, due to the smaller altitude of the airborne with respect to SEASAT, the airborne SAR looking-angle $\theta_a$ changes more rapidly than $\theta_s$ with the ground range $y$ (as a first approximation, $\theta_s$ can be considered constant in a few-hundred meter swath). In other words, the band of the ground reflectivity spectrum collected by SEASAT is almost constant with the ground range, whereas it moves quite rapidly in the airborne case.

The largest ground-range swath $\Delta y$ that allows a partial overlap of the two ground reflectivity spectra can be computed from (6). In fact, the largest allowed spectral shift is $\pm 50$ MHz (in that case we should have a 10 MHz frequency overlap). From (6) (with $\alpha = 0$), the angular separation that corresponds to a $\pm 50$ MHz spectral shift can be computed: $\Delta\theta = \pm .017$ rad. The corresponding ground-range swath is

$$\Delta y = \frac{2H\Delta\theta}{\cos^2 \theta_s} \tag{23}$$

where $H$ is the airborne altitude. If the following values are used:

$$H = 8000 \text{ m}$$

$$\theta_s = 23°$$

a usable swath of about 320 m (or 83 pixels at the airborne sampling spacing) is expected.

Therefore, on the interferogram generated with SEASAT and airborne images we expect to find a rather narrow stripe parallel to the along-track direction where fringes might be detected. It is interesting to note that the only airborne mission requirement that must be strictly fulfilled is that the track direction be as close as possible to that of SEASAT. On the other hand, a very scarce ac-

curacy is requested for the pointing angle (a couple of degrees around the nominal value of 23°) and the track position (some kilometers around the SEASAT-beam center track). Moreover, also a slight deviation of the central frequency would automatically be compensated by a slight change of the looking angle [see again, (6)].

It is easy to appreciate the information given by this experiment: if positive, in desert areas, indeed after multiple airborne surveys and with considerable computer work, one might be able to check the integrated tectonic motions of the last decade.

## IV. Conclusions

The relationship between angular separation and spectral shift has been discussed for the monostatic and bistatic SAR interferometer. This relation has been exploited to improve well-known SAR interferometry techniques and to introduce the idea of the tunable interferometric SAR.

## Acknowledgment

The authors would like to thank the reviewers for their useful suggestions.

## References

[1] R. Graham, "Synthetic interferometer radar for topographic mapping," *Proc. IEEE*, vol. 62, pp. 763–768, June 1974.
[2] A. Gabriel and R. Goldstein, "Crossed orbits interferometry: Theory and experimental results from SIR-B," *Int. J. Remote Sens.*, vol. 9, no. 5, pp. 857–872, 1988.
[3] C. Prati, F. Rocca, A. Monti Guarnieri, and E. Damonti, "Seismic migration for SAR focusing: Interferometrical applications," *IEEE Trans. Geosci. Remote Sens.*, vol. 28, pp. 627–640, July 1990.
[4] E. Rodriguez and J. M. Martin, "Theory and design of interferometric synthetic aperture radars," *IEE Proc., Pt. F*, vol. 139, no. 2, pp. 147–159, 1992.
[5] P. Piau, J-C. Cael, M. Deschaux, and A. Lopes, "Analysis of the resolution of multitemporal SAR systems," in *Proc. IGARSS'93*, Tokyo, Japan, Aug. 1993, pp. 1196–1199.
[6] A. J. Sieber, "The European Microwave Signature Laboratory," *EARSel Adv. Remote Sens.*, vol. 2, no. 1, pp. 195–204, Jan. 1993.
[7] C. Prati and F. Rocca, "Improving slant range resolution of stationary objects with multiple SAR surveys," *IEEE Trans. Aerospace Electron. Syst.*, vol. 29, pp. 135–144, Jan. 1993.
[8] —, "Range resolution enhancement with multiple SAR surveys combination," in *Proc. IGARSS'92*, Houston, TX, May 1992, pp. 1576–1578.
[9] F. Vinelli, "Experimental activities on ERS-1 reference data set," in *Proc. 1st SAR Interferomet. Workshop*, ESA ESRIN, Frascati, Italy, Oct. 12, 1992.
[10] C. Prati and F. Rocca, "Focusing SAR data with time-varying Doppler centroid," *IEEE Trans. Geosci. Remote Sens.*, vol. 30, pp. 550–559, May 1992.

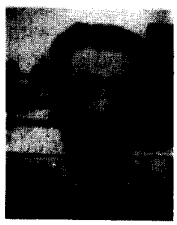

**Fabio Gatelli** was born in Brescia, Italy, on August 4, 1967. He received the "laurea" in electronic engineering from the Politecnico di Milano Milan, Italy, in 1993, with a thesis on innovative applications of SAR (synthetic aperture radar) interferometry.

**Andrea Monti Guarnieri** was born in Milan, Italy, on February 9, 1962. He received the "laurea" in electronic engineering from Politecnico di Milano in 1988, with a thesis on the polyphase DFT filter bank structure applied to synthetic aperture radar data focusing.

He has been with the Department of Electronic Engineering, Politecnico di Milano since 1988, as a member of the SAR research team with Prof. F. Rocca and Prof. C. Prati.

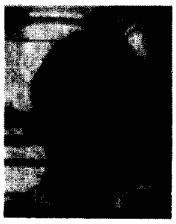

**Francesco Parizzi** graduated in electrical engineering from the Universita' degli studi di Genova in 1990. He is now with Politecnico di Milano, where he is working towards his Ph.D. degree.

His current research interests concern SAR interferometry techniques for DEM generation, small crustal motion estimation, and image resolution improvement.

**Paolo Pasquali** was born in Verbania, Novara, Italy, on November 10, 1965. He received the "laurea" in electronic engineering from the Politecnico di Milano, Milan, Italy, in 1990, with a thesis on biomedical image processing. He is now with the same university, where he is working towards his Ph.D. degree.

His main research interests concern digital processing applied to synthetic aperture radar data, wherein he has studied interferometrical applications and digital elevation maps generation.

**Claudio Prati** received the "laurea" in electronic engineering in 1983, and the Ph.D. degree in 1987, both from the Politecnico di Milano, Milan, Italy.

In 1987 he joined the Centro Studi Telecommunicazioni Spaziali of the National Research Council in Milano. He visited the Department of Geophysics, Stanford University, Stanford, CA, as a Visiting Scholar during the autumn quarter of 1987. Since 1991 he has been an Associate Professor of systems for remote sensing at the Politecnico di Milano.

Prof. Prati was awarded the Symposium Prize Paper Award at the IGARSS'89.

**Fabio Rocca** received the Dottore in Ingegneria Elettronica from the Politecnico di Milano in 1962.

He has worked in the Department of Electronic Engineering of the Politecnico where he is now Professor of Digital Signal Processing. He visited the System Sciences Department at UCLA from 1967 to 1968, and then the Department of Geophysics of Stanford University as Visiting Professor in 1978, 1979, 1981, 1982, 1983, 1986, and, recently, in 1987–

Interim Director of the Stanford Exploration Project. He was Department Chairman in 1975–1978 and, in 1980, was elected to the Commissione d'Ateneo (University Board), where he still serves. He was President of the Osservatorio Geofisico Sperimentale, a National Institute for Research in Geophysics, in 1983–1984. He is currently coordinator of the EEC research program Geoscience, within the Program JOULE. He is also a member of the Scientific Council of the Institut Français du Pétrole. He is an associate editor of the journal *Signal Processing* and has been Associate Editor for seismics of the journal *Geophysical Prospecting* from 1981 to 1985.

He is Past President of the European Association of Exploration Geophysicists and Honorary Member of the Society of Exploration Geophysicists. He was awarded the Honeywell International Award (HUSPI) for biomedical image processing applications in 1979, the Symposium Prize Paper Award at the IGARSS '89, and the Schlumberger award of the EAEG in 1991.